Dynamical surface affinity of diphasic liquids as a probe of wettability of multimodal porous media

J.-P. Korb,[1,*] G. Freiman,[1] B. Nicot,[2] and P. Ligneul[2]
[1]*Physique de la Matière Condensée, Ecole Polytechnique, CNRS, 91128 Palaiseau, France*
[2]*Schlumberger Dhahran Carbonate Research Center, P.O. Box 2836, Al-Khobar 31952, Saudi Arabia*
(Received 18 February 2009; revised manuscript received 29 October 2009; published 1 December 2009)

We introduce a method for estimating the wettability of rock/oil/brine systems using noninvasive *in situ* nuclear magnetic relaxation dispersion. This technique scans over a large range of applied magnetic fields and yields unique information about the extent to which a fluid is dynamically correlated with a solid rock surface. Unlike conventional transverse relaxation studies, this approach is a direct probe of the dynamical surface affinity of fluids. To quantify these features we introduce a microscopic dynamical surface affinity index which measures the dynamical correlation (i.e., the microscopic wettability) between the diffusive fluid and the fixed paramagnetic relaxation sources at the pore surfaces. We apply this method to carbonate reservoir rocks which are known to hold about two thirds of the world's oil reserves. Although this nondestructive method concerns here an application to rocks, it could be generalized as an *in situ* liquid/surface affinity indicator for any multimodal porous medium including porous biological media.

DOI: 10.1103/PhysRevE.80.061601 PACS number(s): 68.08.Bc, 76.60.Es, 81.05.Rm

I. INTRODUCTION

Wettability is the ability of a fluid to spread onto a solid surface in the presence of other immiscible fluids. It is relevant in fundamental interfacial phenomena underlying coating, bonding, adhesion, and other related effects in porous media. For instance, the wettability of a rock/oil/brine system affects fluid saturation, capillary pressures, electrical properties, and relative permeabilities [1–5]. Wettability of fluids in oil and gas reservoirs has a direct effect on efficiency of hydrocarbon recovery. In most cases massive water injection is performed to move oil toward the production zones, and if wettability variations occur the water has the tendency to flow in the water wet locations leaving oil in place in oil-wet locations. Due to its economical impact, control and monitoring of wettability *in situ* justify huge investments in core analysis for laboratory measurements.

Techniques able to map wettability in the field are still not developed. Measurements on cores require long and tedious preparation and never reflect the actual state of wettability. These cores are generally not tested in their native state. They are cleaned and saturated with known brine and oil. They are aged and tested in spontaneous drainage (oil in water saturated core) and imbibition (water in oil saturated core). An Amott index is then determined (from 1 for water wet rocks to −1 for oil wet cores) [6]

A contingent method called USBM (U.S. Bureau of Mines) uses pressure gradient to force the flow of oil in the core saturated with water and reciprocally to force the flow of water in the core saturated with oil [1]. The USBM index (varying for $-\infty$ to $+\infty$) is based on the logarithm of the ratio of energy required to move oil with water versus the energy required to move water with oil. Both Amott and USBM methods are accepted as a standard by industry; however, they do not completely compare in all cases [7]. A direct measurement of wettability between rocks oil and brine can be done in laboratory by drop shape analysis (DSA) using pure flattened samples of nonporous rocks and oil and brine. This method is valid when the measurement is localized (drop diameter in the range of 10 μm to 1 mm) and the fluids have to be stable (no gas diffusion or surfactant migration during experiments) [2]. The method for instance is very well adapted for analyzing the effect of wettability modifiers in rock/oil/water systems. However, porous rocks cannot be tested directly by DSA. Amott, USBM, and DSA methods cannot be carried out in the well. A more recently introduced NMR T_2 index [8–10] expresses the total surface of rock wetted by water minus the total surface of rock wetted by oil and divided by the total surface in contact with the fluid. This method uses the fact that a fluid surrounded by a wetting fluid shows a T_2 relaxation distribution of a bulk fluid, whereas a fluid in contact with the rock exhibits a shorter T_2 due to the confinement by the surface. This method has some limitations since it requires a measurement at complete water saturation and also requires the knowledge of the T_2 shape of the oil in bulk conditions. None of these techniques allow the local probing of interaction between the fluid and the rock-pore surface in a single noninvasive measurement.

Here, we propose to use nuclear magnetic relaxation dispersion (NMRD) [11,12] to probe the dynamical surface affinity of diphasic liquids as a measurement of wettability. This technique measures proton $1/T_1$ over a large range of applied magnetic fields and yields unique information about the extent to which a fluid is dynamically correlated with a solid rock surface. Unlike conventional transverse relaxation studies [8,13], this approach is a direct probe of the dynamical surface affinity of fluids [14,15]. We show that the low-frequency dispersion of the proton spin-lattice relaxation rates $1/T_1$ of aprotic (oil) and protic (water) diphasic liquids can provide their relative wettabilities in porous media with complex pore-size distribution (multimodal). The use of aprotic and protic liquids allows studying the physical chemistry effects that matters at pore surface such as binding ef-

*Corresponding author; jean-pierre.korb@polytechnique.fr

 ©2009 The American Physical Society

fects with paramagnetic metallic ions or proton exchange with surface groups.

We predict theoretically the specific NMRD features of aprotic liquids diffusing in the proximity of paramagnetic relaxation sites at pore surfaces and protic liquids bounded to these sites. To quantify these features we introduce a microscopic dynamical surface affinity index which measures the dynamical correlation (i.e., the microscopic wettability) between the diffusive fluid and the fixed relaxation sources at the pore surfaces. We apply this noninvasive *in situ* method to carbonate reservoir rocks of bimodal porosity which are known to hold about two thirds of the world's oil reserves [16]. We confirm experimentally the predictions of the relaxation features for aprotic and protic liquids as well as pore-size dependence of wettability. The *in situ* results obtained on carbonates of bimodal porosity saturated with an oil/brine mixture reveal unambiguously the pore-size dependence of wettability. Although this method concerns here an application to rocks, it could be generalized as an *in situ* liquid/surface affinity indicator for any multimodal porous medium including porous biological media.

II. SAMPLES AND METHODS

A. Samples

The rock samples used here are carbonate rocks from a Middle Eastern oil reservoir. They are intraclast skeletal ooid grainstone carbonates with 30% porosity and 700 mD permeability. A thin section observed by polarized microscopy [Fig. 1(a)] reveals the complex structure of this rock formed by grains partially dissolved and coated by calcite cement. This rock is formed of medium to very coarse grains; those grains are oolites, coated grains, intraclasts, gastropods, or forams. The macroporosity, evidenced in gray in the thin section [Fig. 1(a)], has a pore size ranging from 2 mm to 50 μm. Microporosity, however, is not visible from thin section images, but the dual porosity of this rock is evidenced by the bimodal T_1 distribution obtained both by a one-dimensional (1D) Laplace inversion method and an iterative multiexponential decomposition of the longitudinal magnetization decay of brine at 15 MHz [Fig. 1(b)]. This shows large pores corresponding to T_1 relaxation time on the order of 400 ms and microporosity corresponding to T_1 on the order of 30–40 ms.

This rock was sampled into cylindrical plugs of 8 mm in diameter and 10 mm in length. The homogeneity of the rock at the plug scale allows comparing results from different plugs. Originally, the rock plugs are filled with native fluids; this is called "native state." They were cleaned using a standard cleaning procedure in a petrophysical laboratory using toluene and methanol in a Soxhlet extractor to remove all the native fluids inside the rock (original crude oil and brine). Three rock plugs were then dried in an oven at 60 °C for 48 h and each of them prepared at a different saturation:

(i) 100% water saturation (S_w=100%): this plug was vacuumed and saturated with a 50 kppm NaCl brine. The use of salty water prevents dissolution of the carbonate rock by fresh water.

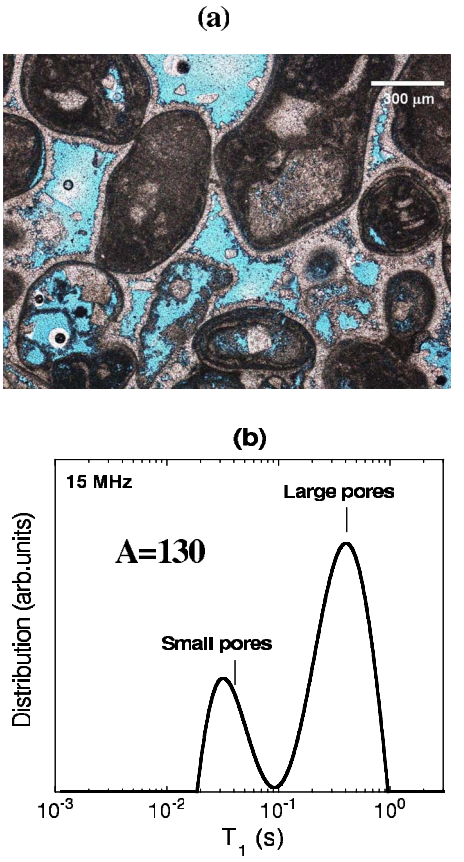

FIG. 1. (Color online) (a) Thin rock section of the studied intraclast skeletal ooid grainstone of 30% porosity and 700 mD permeability as seen by polarized optical microscopy. (b) Dual porosity observed through the T_1 distribution obtained by the 1D Laplace inversion of the longitudinal magnetization decay of brine at 15 MHz. The vertical ticks represent the two T_1 values deduced from the iterative multiexponential approach.

(ii) 100% dodecane saturation (S_w=0%): this plug was vacuumed and saturated with dodecane and said to be at 0% water saturation (S_w=0%).

(iii) Irreducible water saturation S_{wirr}: this plug is first saturated 100% with water, then dodecane is forced into the plug by high speed centrifugation. The density difference between dodecane and brine forces dodecane to replace brine in the pore space. This plug is said to be at irreducible water saturation (S_w=S_{wirr}).

B. Methods

The proton NMRD data were recorded using a fast field cycling (FFC) NMR spectrometer from Stelar s.r.l., Mede, Italy. We used a fast field cycling sequence to improve the signal-to-noise ratio, where spins are polarized at 15 MHz and the free-induction decays are recorded following a single 90° excitation pulse of 5.8 μs duration applied at 11 MHz. The temperature was fixed at 298 K. The experiment was performed over a large range of proton Larmor frequencies (10 kHz–20 MHz) in order to obtain the complete dispersion curve of $1/T_1$.

Electron spin resonance (ESR) spectroscopy at room temperature was used to determine the nature and the quantity of paramagnetic impurities in our carbonate samples. On a dry sample, we observe the six-peak hyperfine structure centered on $g=2$ characteristic of electronic spins $S=5/2$ of paramagnetic Mn^{2+} ion in a single environment. This spectrum is a result of Mn^{2+} substituting for Ca^{2+} in a single site of trigonal symmetry having as its nearest neighbors six-carbonate ions in the carbonate crystal lattice. There exists a broad line underneath the Mn^{2+} ESR spectrum. This could be attributed to magnetic Fe^{3+} impurities in the dolomite crystals filling between grains and inside molts. We have calibrated the ESR surface area by measuring the signal in the presence of a definite amount of monocrystals of $CuSO_4$, $5H_2O$ diluted in KBr powder. This has allowed us to measure a volume density $\eta_S=8.4\times10^{19}$ Mn^{2+} ions per gram of sample. We describe in Appendixes A and B how we deduce from η_S a homogeneous surface density $\sigma_S=1.05\times10^{13}$ Mn^{2+}/cm^2 within a thin layer $\xi\sim0.5$ nm of paramagnetic ions corresponding to the lattice constant of the calcium carbonate lattice structure at proximity of the pore surface. We show in the following that only such a layer of paramagnetic impurities at pore surfaces will be active on the NMRD of liquid proton species moving at proximity.

Concerning the influence of possible heterogeneous Mn^{2+} concentrations in different length scales, we have compared our NMRD data with the ones observed on another fully saturated packstone carbonate sample of lower porosity, pore size, and permeability that presents differences in chemical composition. Fujiwara [17] has shown that ESR spectra could change progressively from a six-peak hyperfine structure to a very broad inhomogeneous spectra when increasing the density of Mn largely above the density η_S value that we found. In this packstone carbonate of smaller porosity, we observe only the six-peak hyperfine structure with a much less quantity of Mn^{2+} and we do not observe any large variation in the NMRD data compared to the ones described in this work on the grainstone carbonate. These observations thus exclude the possibility that heterogeneous concentration or clusters of Mn are at the origin of the observed NMRD data.

III. NMRD EXPERIMENTS OF APROTIC AND PROTIC LIQUIDS IN CARBONATE ROCKS

A. How to probe dynamical surface effects by proton NMRD in macropores?

The physical aspect of this study is the possibility to map the wettability from surface dynamical parameters extracted from critical proton NMRD features, $R_1(\omega)=1/T_1(\omega)$, either for monophasic or diphasic (aprotic and protic) liquids in macroporous rocks. Such a possibility is based on the following physical arguments.

(i) In the fast diffusion limit, one can apply the biphasic fast exchange model where the exchange time between the surface and the bulk phases is shorter than their respective relaxation times; the overall proton relaxation rate $1/T_1$ is thus a linear combination of a bulk $1/T_{1,bulk}$ and a surface relaxation rate $1/T_{1,surface}$ [14].

(ii) Even if we measure the bulk longitudinal magnetization decay, due to the very large paramagnetic moments of the few paramagnetic impurities at the pore surface, one has the relation $T_{1,surface}\ll T_{1,bulk}$ involving that the surface term dominate the NMRD especially at low frequency.

(iii) The magnetic-field dependence of the nuclear spin relaxation rate is a rich source of dynamical information especially for confined liquids. Varying the magnetic field changes the Larmor frequency, and thus, the fluctuations to which the nuclear spin relaxation is sensitive. Further, the magnetic-field dependence of the spin-lattice relaxation rate, $1/T_1$, provides a good test of the theories that relate the measurement to the microdynamical behavior of the liquid. This is especially true in highly spatially confined systems where the effects of reduced dimensionality may force more frequent reencounters of spin-bearing molecules either with paramagnetic ions or with proton-surface groups. These reencounters alter the correlation functions which directly govern the relaxation equations.

(iv) The local chemical properties at proximity of the surface relaxation sink will be largely enhanced by such molecular reencounters. Depending on the different possibilities of proton exchange of the studied liquid, there will be some critical surface NMRD $1/T_{1,surface}(\omega)$ profiles allowing to discriminate dynamically the nature of the liquid at (or at proximity) of the pore surface.

(v) We show below that one observes two NMRD profiles, $R_{11}(\omega)$ and $R_{12}(\omega)$, corresponding to the two means of the peaks of the bimodal distribution of the overall longitudinal relaxation rates. In all the cases, we succeed to renormalize these data in a single master NMRD profile. This rescaling of the data proves unambiguously the universality of the relaxation model in each case. We will detail in Sec. IV the relevant theoretical models that allow us to extract the surface dynamical parameters from the frequency dependence of such rescaling NMRD data without the numerous parameters usually encountered in NMR.

In the following, we present the proton NMRD data of oil and/or water in carbonate rocks in the three different saturations described in Sec. II A. The discussion of the fitting procedure allowing the extraction of the surface dynamical parameters is reported in the theoretical Sec. IV.

B. NMRD in the case of monophasic saturation with aprotic dodecane ($S_w=0\%$)

The NMRD data obtained in the case of a monophasic saturation of carbonate rocks with aprotic dodecane are shown in Fig. 2(a). We observe bilogarithmic frequency dependences of the two spin-lattice relaxation rates $R_{11}=1/T_{11}$ and $R_{12}=1/T_{12}$ corresponding to the two peaks of the T_1 distribution [Fig. 1(b)]. Owing to the constant value of the affinity ratio, $R_{12}(\omega_I)=4R_{11}(\omega_I)$, within all the frequency ranges studied, we successfully rescaled these proton-dodecane NMRD data onto a single bilogarithmic master curve [inset of Fig. 2(a)]. This rescaling unambiguously proves the existence of a unique relaxation mechanism. We show in Sec. IV B that the frequency behavior observed in the inset of Fig. 2(a) is typical of an intermolecular dipolar

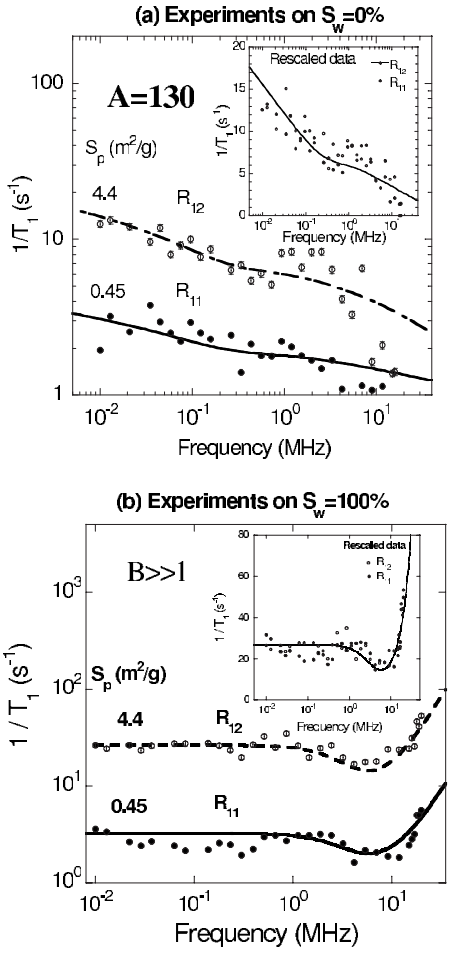

FIG. 2. (a) Measured NMRD of carbonate rock saturated with dodecane (S_w=0%). Here $R_{11}=1/T_{11}$ and $R_{12}=1/T_{12}$ represent the relaxation rates obtained from a biexponential decay of the longitudinal magnetization corresponding to two pore sizes. The continuous lines were obtained from Eqs. (6) and (7) without the $1/T_{1,param}(\omega_I)$ contribution leading to the surface dynamical affinity $A=130$. The inset shows the rescaled data on a single master curve. (b) Measured NMRD of carbonate rock saturated with 50 kppm NaCl brine (S_w=100%). The continuous lines were obtained from Eqs. (8)–(10) without the $1/T_{1,2D}(\omega_I)$ contribution leading to $B \gg 1$. The inset shows the rescaled data on a single master curve.

relaxation mechanism for the NMRD data of R_{11} and R_{12} modulated by the translational 2D diffusion of aprotic dodecane molecules that diffuse at proximity of paramagnetic impurities at coarse grained pore surfaces.

C. NMRD in the case of monophasic saturation with protic brine (S_w=100%)

The NMRD data obtained in fully brine-saturated carbonate rocks are shown in Fig. 2(b). Here again, we observe two spin-lattice relaxation rates R_{11} and R_{12}. We also successfully rescaled these NMRD water data onto a single master curve [inset of Fig. 2(b)], thereby limiting the number of free parameters necessary to fit the data. Owing to the constant value of the affinity ratio, $R_{12}(\omega_I) \sim 8R_{11}(\omega_I)$, within all the frequency ranges studied, we successfully rescaled the NMRD data in the inset of Fig. 2(b). This affinity ratio is twice the one observed for dodecane in the inset of Fig. 2(a). We will show in Sec. IV C that the relaxation process at the origin of these NMRD data is the nuclear paramagnetic relaxation of water molecule bonded on the ligand field of the metallic paramagnetic ion at the pore surfaces. The net enhancement of the ratio R_{12}/R_{11} can be explained by the fact that water approaches more closely the very convoluted surface of the carbonate.

D. Diphasic saturation with aprotic dodecane and protic brine (S_{wirr})

The NMRD data obtained in the case of a diphasic mixture saturating the carbonate rocks with both dodecane and brine are shown in Fig. 3(a). The relaxation rates of the mixture (large full dots) are compared with the rates R_{11} and R_{12} (small empty dots) obtained with monophasic saturations of dodecane [S_w=0%, data taken from Fig. 2(a)] and water [S_w=100%, data taken from Fig. 2(b)], respectively. Here, R_{11} has the typical NMRD signature of dodecane in large pores [Fig. 2(a)], whereas R_{12} exhibits the typical NMRD signature of brine in small pores [Fig. 2(b)]. These results thus reveal a clear identification of the nature of the liquids saturating the dual porosity of carbonate observed through the T_1 distribution obtained by a 1D Laplace inversion of the longitudinal magnetization decay at 15 MHz shown in Fig. 3(b). Integrating this distribution gives a water saturation of 20% that is independent of frequency [Fig. 3(c)]. Because we saturated the cores with water first, it is indeed expected that water preferably fills the small pores and dodecane the large ones. However, in a general case of native states samples, there is no known such preferred pattern. The proposed methodology allows identification of the two embedded liquids through their dynamical surface behaviors. The similarity between the T_1 distribution at S_w=100% [Fig. 1(b)] and S_{wirr} [Fig. 3(b)] for the studied rock reveals that dodecane has successfully invaded the large pores without entering the small ones. This proves the existence of flow path between the large pores that does not involve the small pores. In this case, the two-pore systems can be viewed as parallel systems explaining the high permeability found for this rock (700 mD). This is an important result that explains the different wetting behaviors of oil and brine in differently sized pores.

IV. THEORY AND DISCUSSION OF EXPERIMENTAL NMRD RESULTS

A. Biphasic fast exchange in macroporous rocks

In the fast diffusion limit, one can apply the biphasic fast exchange model where the exchange time between the surface and the bulk phases is shorter than their respective relaxation times; the overall proton relaxation rate $1/T_1$ is a linear combination of a bulk $1/T_{1,bulk}$ and a surface relaxation rate $1/T_{1,surface}$. We show here that the surface term is a superposition of the contribution $1/T_{1,2D}$ of the proton species diffusing in the proximity of the fixed paramagnetic species and the contribution $1/T_{1,param}$ of the proton species

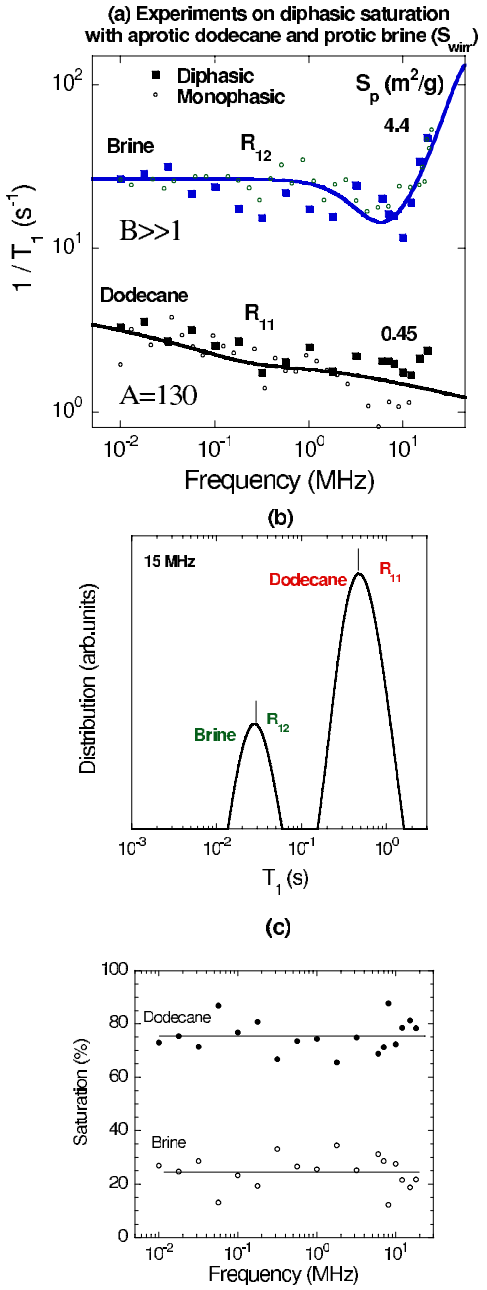

FIG. 3. (Color online) (a) Measured NMRD of carbonate rock saturated with both dodecane and 50 kppm NaCl brine ($S_{w,irr}$). The continuous lines were obtained from Eqs. (6) and (7) for dodecane (aprotic) leading to the surface dynamical affinity $A=130$ and from Eqs. (8)–(10) for wetting brine leading to $B \gg 1$. The relaxation rates of the mixture (large full dots) are compared with the rates R_{11} and R_{12} (small empty dots) obtained with monophasic saturations of dodecane [data taken from Fig. 2(a)] and brine [data taken from Fig. 2(b)], respectively. (b) Dual porosity observed through the T_1 distribution obtained by the 1D Laplace inversion of the longitudinal magnetization decay at 15 MHz. The vertical ticks represent the two T_1 values deduced from the iterative approach. The comparison with the NMRD data allows to identify the nature of the liquid saturating individual pore. (c) Frequency dependence of the saturation (%) of brine and dodecane that is conserved in the whole frequency range studied. This saturation has been obtained by integration of the bimodal distribution at each frequency.

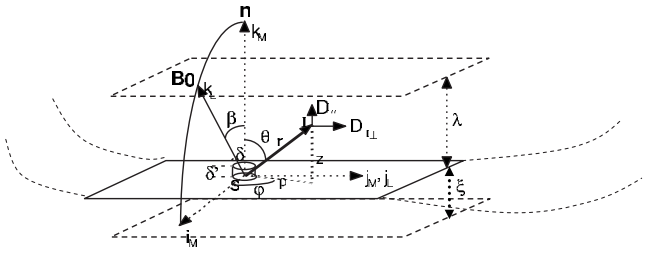

FIG. 4. Schematic of the layer model. The nuclear spins I diffuse in an infinite layer of thickness λ in the dipolar field of a very small quantity of paramagnetic spins S fixed on the surface. The M axes are fixed in the layered system. The L axes are fixed in the laboratory frame, with the constant magnetic field $\boldsymbol{B}_0$ at the angle β from the normal axis $\boldsymbol{n}$. The relative cylindrical polar coordinates ρ, φ, and z are based on the M frame. The smallest value of ρ and z corresponding to the distance of minimal approach of the two I- and S-spin-bearing molecules at the surface is δ'. The distinctions between the translational diffusion constants of spin I are indicated on the diagram.

linked to the first coordination sphere of paramagnetic centers [18]:

$$\frac{1}{T_1(\omega_I)} = \frac{1}{T_{1,bulk}} + \frac{N_{surface}}{N}\frac{1}{T_{1,2D}(\omega_I)} + \frac{N_{param}}{N}\frac{1}{T_{1,param}(\omega_I)}. \tag{1}$$

The bulk relaxation term, $1/T_{1,bulk}$, has no proton Larmor frequency $\omega_I/2\pi$ dependence in the range studied here [19]. The two surface relaxation terms are highly sensitive to the local physical-chemistry effects at the pore surface resulting in different frequency behaviors in disconnected ranges. The inclusion of the nuclear paramagnetic term is critical because it extends the theory to make the NMRD of protic liquid different to the aprotic one. We proposed below to calculate these two terms in the local layer geometry at proximity of the pore surface (Fig. 4). In this model, $N_{surface}/N = \lambda S_P \rho_{liquid}$ is the ratio between the number of liquid molecules diffusing within the thin transient layer λ close to the pore surface and in the bulk (Fig. 4); λ is of the order of a few molecular sizes [20]. S_p is the specific surface area of the rock and ρ_{liquid} is the density of the proton liquid. $N_{param}/N = (N_{param}/N_S)(N_S/N) \ll N_S/N$ is the ratio between the number of liquid molecules bonded to the paramagnetic sites at the surface and in the bulk.

The paramagnetic sites located at the pore surface have a ligand field which either traps a moving proton species [defined as a *protic* liquid wetting the surface; inset of Fig. 5(b)] or does not trap a moving proton species [defined as an *aprotic* liquid wetting the surface, or, a *protic* liquid not in direct contact with the surface; inset of Fig. 5(a)]. These chemical behaviors result in two distinct features of the NMRD that can be individualized by $1/T_{1,2D}(\omega_I)$ or $1/T_{1,param}(\omega_I)$ in Eq. (1) in the case of monophasic saturation and used as a liquid recognition criterium for a diphasic saturation. We propose to use these features to determine the wettability of dodecane (aprotic) and water (protic) in carbonate rocks.

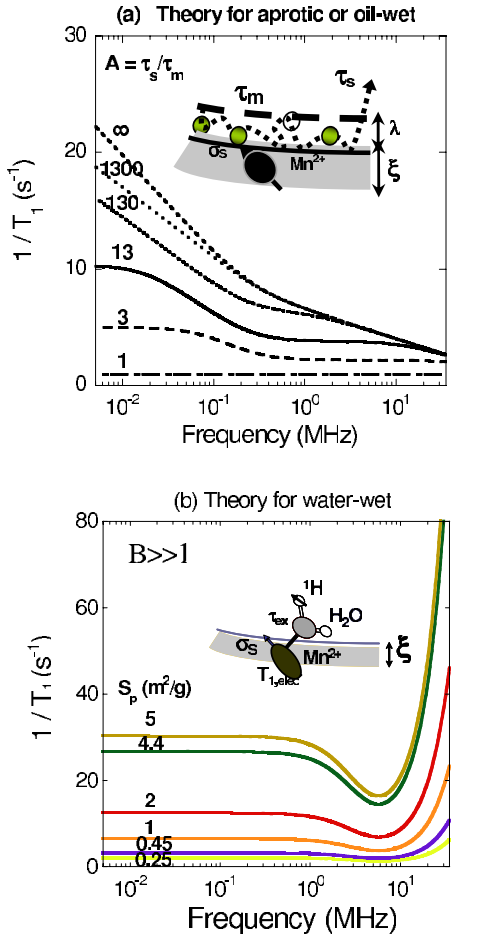

FIG. 5. (Color online) (a) Typical examples of theoretical NMRD for aprotic dodecane calculated with Eqs. (6) and (7) using typical values corresponding to dodecane in a carbonate rock: $S_p = 4.4$ m^2/g, $\tau_m = 1$ ns, and increasing values of the surface dynamical affinity $A = \tau_S/\tau_m$ from 1 (bulk value) to ∞ (unlimited surface area). The inset shows a schematic of a quasi-2D diffusion relaxation model of an aprotic (or oil-wet) liquid diffusing at the proximity of the pore surface. (b) Typical examples of theoretical NMRD data calculated using Eqs. (8)–(10) for water when varying S_p and $B \gg 1$. The inset shows a schematic of a nuclear paramagnetic relaxation of water bonded to the ligand field of Mn^{2+} at the pore surface (water-wet condition).

B. Theory and discussion of NMRD data in the case of monophasic saturation with aprotic dodecane

We first consider the case of $1/T_{1,2D}(\omega)$ corresponding to proton bearing aprotic liquid diffusing in proximity to the solid liquid interface in a porous rock; i.e., the proton species is not trapped in the ligand field of a paramagnetic site. This allows not considering the $1/T_{1,param}(\omega_I)$ contribution in Eq. (1). We consider also the presence of a very small quantity of fixed paramagnetic species of spins, S, uniformly distributed on these surfaces with a surface density, σ_s. Because the magnetic moment of the paramagnetic species is large ($\gamma_S = 659\gamma_I$), there is no ambiguity about the relaxation mechanism of the diffusing proton spins, I, which is the intermolecular dipolar relaxation process induced by fixed spins, S, and modulated by the translational diffusion of the mobile spins, I, in close proximity to these surfaces. Basically, the nuclear spin-lattice relaxation rate of the diffusing spins I, in proximity to the S spins, is given formally by the general expression

$$\frac{1}{T_{1,2D}(\omega_I)} = \frac{2}{3}(\gamma_I\gamma_S\hbar)^2 S(S+1)\left[\frac{1}{3}J_L^{(0)}(\omega_I-\omega_S) + J_L^{(1)}(\omega_I) + 2J_L^{(2)}(\omega_I+\omega_S)\right], \tag{2}$$

where $J_L^{(m)}(\omega)$ $(m \in \{-2,+2\})$ are the spectral densities in the laboratory frame (L) associated with the constant magnetic field $\boldsymbol{B}_0$ (Fig. 4) expressed at the Larmor frequencies of the electron and proton related by $\omega_S = 658.21\ \omega_I$ and defined as the exponential Fourier transforms,

$$J_L^{(m)}(\omega) = \int_{-\infty}^{+\infty} G_L^{(m)}(\tau)e^{-i\omega\tau}d\tau, \tag{3}$$

of the stationary pairwise dipolar correlation functions $G_L^{(m)}(\tau)$ $(m \in \{-2,+2\})$ given by

$$G_L^{(m)}(\tau) = \langle F_L^{(-m)}(t)F_L^{(-m)*}(t+\tau)\rangle. \tag{4}$$

Equation (4) describes the persistence of the autocorrelation of the dipole-dipole interaction $F_L^{(m)}(t) \sim 1/r_{IS}^3(t)$ between the magnetic moments associated with the spins I and S and modulated by the translational diffusion during a short time interval τ of spins I at distance r_{IS} of a paramagnetic spins fixed on the pore surface. The notation $\langle \ldots \rangle$ stands for the ensemble average over all the positions of the spins I at time 0 and τ for a given density σ_S of spins S. This ensemble average can be expressed as an integral average over the normalized diffusive propagator $P(\vec{r}_0, \vec{r}, \tau)$:

$$G_L^{(m)}(\tau) = \int d\vec{r}_0 p(\vec{r}_0)F_L^{(-m)}(0)\int d\vec{r}P(\vec{r}_0,\vec{r},\tau)F_L^{(-m)*}(\tau). \tag{5}$$

Here $P(\vec{r}_0, \vec{r}, \tau)$ is a solution of a diffusive equation with initial and boundary conditions and $p(\vec{r}_0) = \sigma_S/\lambda$ represents the equilibrium and uniform density of spin pairs I-S at equilibrium.

We have detailed in Appendix A all the calculations of the correlation functions $G_L^{(m)}(\tau)$ and spectral densities $J_L^{(m)}(\omega)$ within the following conditions. (i) We use the well known properties of rotation of spherical harmonics in different bases to facilitate the calculations in the lamellar frame (M) of Fig. 4 before coming back to the laboratory frame (L) associated to the constant direction of the magnetic field $\boldsymbol{B}_0$. (ii) We use the anisotropic dynamical model presented in Fig. 4 with an unbounded and isotropic diffusion perpendicular to the normal axis $\boldsymbol{n}$ and a bounded diffusion along such an axis. (iii) The pairwise dipolar correlation functions $G_L^{(m)}(\tau)$ have been estimated at times τ much longer than the transverse diffusion correlation time $\tau_m = \delta^2/(4D_{I\perp})$, where δ is the molecular size of the I spin-bearing molecule with a translational diffusion coefficient $D_{I\perp}$ in direction perpendicular to $\boldsymbol{n}$. (iv) We introduce the effects of the finite time of residence $\tau_S \gg \tau_m$ at pore surface by an exponential cutoff in

the time dependence of the pair correlations *IS*. (v) A powder average of $J_L^{(m)}(\omega)$ over all the orientations of the $\boldsymbol{n}$ direction relative to the constant direction of the magnetic field $\boldsymbol{B_0}$ has been done.

Substituting Eq. (A11) into Eq. (2) leads, at low frequency, to the spin-lattice relaxation rate of the 2D diffusion of dodecane diffusing in proximity to the pore surface:

$$\frac{1}{T_{1,2D}(\omega_I)} = \frac{\pi}{30}\langle\omega_d^2\rangle\tau_m\left[3\ln\left(\frac{1+\omega_I^2\tau_m^2}{(\tau_m/\tau_s)^2+\omega_I^2\tau_m^2}\right) + 7\ln\left(\frac{1+\omega_S^2\tau_m^2}{(\tau_m/\tau_s)^2+\omega_S^2\tau_m^2}\right)\right]. \quad (6)$$

Finally, substitution of Eq. (6) into Eq. (1) reduced to the superposition of the bulk and only the 2D surface contributions gives for the spin-lattice relaxation rate $1/T_{1,aprotic}(\omega_I)$ of an aprotic liquid (dodecane) diffusing in proximity to the pore surface in the presence of paramagnetic impurities:

$$\frac{1}{T_{1,aprotic}(\omega_I)} = \frac{1}{T_{1,bulk}} + \frac{N_{surface}}{N}\frac{1}{T_{1,2D}(\omega_I)}. \quad (7)$$

In Eq. (6), we have introduced the quadratic static dipole-dipole frequency $\langle\omega_d^2\rangle=[\sigma_S/(x^2\lambda^2\delta'^2)](\gamma_I\gamma_S\hbar)^2S(S+1)$ between I and S spins of gyromagnetic ratios γ_I and γ_S averaged over the layered geometry λ. $x=\delta/\delta'$ is a parameter introduced in Appendix A for taking into account a variable distance δ' of minimal approach between spins I and S compared to the molecular size δ. $S=5/2$ for the spin of Mn^{2+} paramagnetic ions of concentration $\eta_S=8.4\times10^{19}$ Mn^{2+}/g measured on a representative carbonate rock by ESR and we show in Appendix B that $\sigma_S=(\eta_S\rho_{solid}\xi)=1.05\times10^{13}$ Mn^{2+}/cm^2. Equation (6) has a bilogarithmic frequency dependence (proton Larmor frequency ω_I and electronic frequency $\omega_S=659\omega_I$) due to the numerous 2D molecular reencounters between spins I and S occurring within the thin transient layer λ. Equation (6) contains two correlation times: the translational correlation time, τ_m, associated with individual molecular jumps in proximity to the surface and the surface residence time, τ_s, which is limited by the molecular desorption from the thin surface layer λ. τ_s controls how long the proton species I and the Mn^{2+} ion S stay correlated. It depends on both the strength of the chemical bonds and the reoccurrence of first neighbor interactions induced by the fluid confinement in pores.

Surface dynamical affinity and introduction of a NMR T_1 wettability index

We introduce a microscopic dynamic surface correlation parameter $A=\tau_s/\tau_m$ (affinity index) in lieu of the more traditional and loosely defined macroscopic wettability indices. The index A represents roughly the average number of diffusing steps of spins I in proximity to fixed paramagnetic sites S during the time scale of a NMRD measurement [inset of Fig. 5(a)]. The larger this index, the more numerous the 2D reencounters are and, therefore, the more correlated the I-S spins. As such, A reveals the affinity of the fluid to the pore surface, i.e., the microscopic wettability.

The successful rescaling of the proton-dodecane NMRD data onto a single bilogarithmic master curve [inset of Fig. 2(a)] proves unambiguously that a unique relaxation process is responsible for the NMRD data of R_{11} and R_{12} and that the difference of a factor 4 between the NMRD of R_{11} and R_{12} is solely a result of the prefactors in Eq. (7), namely, the specific surface area S_p associated to the different pore sizes. The theoretical curves displayed in Fig. 5(a) show the results of the calculation of $1/T_{1,aprotic}(\omega_I)$ [Eq. (7)] with $\tau_m=1$ ns and with increasing values of A from 1 to ∞. When $A=1$, $1/T_{1,aprotic}(\omega_I)$ reduces to $1/T_{1,bulk}$ which is characteristic of the bulk case without any surface affinity. When $A->\infty$, we reach the case of a pure oil-wet condition for *aprotic* dodecane. In that case, the theoretical NMRD has a bilogarithmic form with a ratio of 10/3 between the two slopes at low and high frequency. In between these two latter values of A, one notes some plateau in the theoretical NMRD at low and intermediate frequency range [Fig. 5(a)]. The dynamical parameters $\tau_m=1.0$ ns and $\tau_s=130$ ns can straightforwardly be obtained, with a very good accuracy, from the frequency dependences of the rescaled data [inset of Fig. 2(a)], without involving all of the parameters required in Eqs. (6) and (7). These dynamical correlation times result in an affinity index of $A\sim130$, which corresponds to a weak dynamical affinity (small time of residence at pore surface) of the carbonate surface for aprotic dodecane.

C. Theory and discussion of NMRD data in the case of monophasic saturation with protic brine

We now consider the case of $1/T_{1,param}$ corresponding to proton bearing (water) staying in the ligand field of the paramagnetic ions for a time τ_{ex} longer than the surface or bulk correlation times [inset of Fig. 5(b)]. The nuclear paramagnetic relaxation rate is given by [21,22]

$$\frac{1}{T_{1,param}(\omega_I)} = \frac{2}{15}\omega_{d,IS}^2 T_{1,elec}(\omega_S)\{3/[1+\omega_I^2T_{1,elec}^2(\omega_S)] + 7/[1+\omega_S^2T_{1,elec}^2(\omega_S)]\}. \quad (8)$$

The quadratic dipole-dipole frequency $\omega_{d,IS}^2=(\gamma_I\gamma_S\hbar/\delta'^3)^2S(S+1)$ represents now the interaction between a proton-water and a given Mn^{2+} ion at a distance of minimal approach $\delta'=0.27$ nm. The frequency dependence of Eq. (8) is a sum of two Lorentzian spectral densities at frequencies ω_I and ω_s. The electronic correlation time $T_{1,elec}(\omega_S)$ depends on the magnetic field through the electronic frequency ω_S [21,22]:

$$\frac{1}{T_{1,elec}(\omega_S)} = H_S^2\tau_v\left[\frac{1}{1+\omega_S^2\tau_v^2}+\frac{4}{1+4\omega_S^2\tau_v^2}\right], \quad (9)$$

where τ_v is the correlation time for the electron-lattice fluctuating interaction and H_S^2 is the intensity of the electron-spin fluctuations [22] and typically $T_{1,elec}(\omega_S)\approx10^{-10}$ s for Mn^{2+} when $\tau_{ex}\gg T_{1,elec}$. Equations (8) and (9) are very well known from the magnetic resonance imaging [23] in which Mn(II) ions or Gd(III) ions are used as contrast agents.

Substitution of Eqs. (8) and (9) into Eq. (1) reduced to the superposition of the bulk and paramagnetic contributions

[without the $1/T_{1,2D}(\omega_I)$ contribution], i.e., gives the following expression for a protic spin-lattice relaxation rate in macropores:

$$\frac{1}{T_{1,protic}(\omega_I)} = \frac{1}{T_{1,bulk}} + \frac{N_{param}}{N}\frac{1}{T_{1,param}(\omega_I)}, \qquad (10)$$

where $N_{param}/N=(\lambda S_P \rho_{liquid})\delta^2\sigma_S f \ll N_S/N$ is the ratio between the number of liquid molecules bonded to the paramagnetic sites at the surface and in the bulk; $\delta=0.3$ nm is the mean molecular size of water. f is a geometrical factor that takes into account the increase in accessibility of water to the paramagnetic relaxation sink on the very convoluted surface of carbonate rocks. In this case the water molecule has a strong correlation with the relaxing elements on the rock surface (representing a water-wet condition). We show in Appendix B that $\sigma_S=(\eta_S\rho_{solid}\xi)=1.05\times10^{13}$ Mn^{2+}/cm^2, where the paramagnetic concentration $\eta_S=8.4\times10^{19}$ Mn^{2+}/g is measured on a representative carbonate rock by ESR. ρ_{solid} is the density of the carbonate rock and the length scale $\xi\sim0.5$ nm is the thickness of the relaxing surface distribution of Mn^{2+} ions corresponding to the lattice constant of the calcium carbonate lattice structure at proximity of the pore surface (Fig. 4). Typical examples of theoretical NMRD calculations, varying the specific surface area S_p, are displayed in Fig. 5(b) which show the characteristic features of a plateau at low frequency and a peak above 10 MHz.

An experimental illustration of nuclear paramagnetic relaxation NMRD behavior is obtained with our carbonate sample now saturated with brine. We observe two spin-lattice relaxation rates R_{11} and R_{12} [Fig. 2(b)]. Due to the ratio of the two NMRD, $R_{12}(\omega_I)/R_{11}(\omega_I)\sim8$, we successfully rescaled these NMRD water data onto a single master curve [inset of Fig. 2(b)], thereby limiting the number of free parameters in Eq. (10). The net enhancement of the affinity factor $R_{12}(\omega_I)/R_{11}(\omega_I)$ can be explained by the fact that water approaches more closely the very convoluted surface of the carbonate rock.

One could define also an index $B=\tau_{ex}/T_{1,elec}(\omega_S)$ by comparing the time of residence τ_{ex} on the paramagnetic ions to the electronic spin-lattice relaxation time $T_{1,elec}(\omega_S)$. In the nuclear paramagnetic relaxation case considered, the best fit is obtained with $T_{1,elec}=8.6\times10^{-11}$ s, validating the initial assumption $\tau_{ex}\gg T_{1,elec}$ so $B\gg1$ which explains the net increase of $1/T_{1,protic}(\omega_I)$ at large frequencies. In the opposite case where $B<1$, $1/T_{1,protic}(\omega_I)$ decreases at large frequencies, as it is observed in the case of paramagnetic impurities fixed on proteins in solution [23].

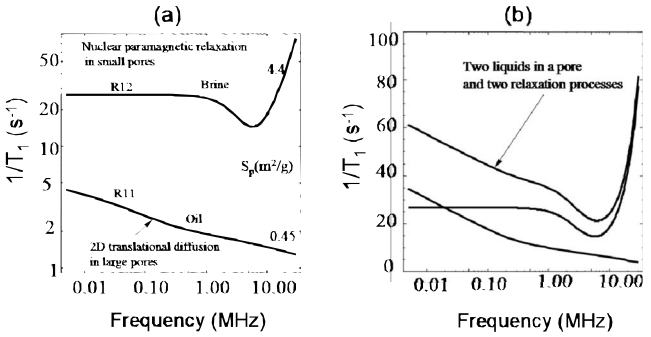

FIG. 6. (a) Theoretical NMRD profiles for aprotic dodecane calculated with Eqs. (6) and (7) in large pores and calculated with Eqs. (8)–(10) for protic brine in small pores. (b) Theoretical NMRD profiles calculated with Eqs. (6)–(10) in the case of dodecane and brine in the same pore in the condition of mixed wettability. We have displayed the individual contributions of the two-dimensional diffusion [Eqs. (6) and (7)], the nuclear paramagnetic relaxation process [Eqs. (8)–(10)], as well as the superposition of these two relaxation processes [Eq. (11)].

D. Theory and discussion of NMRD data in the case of diphasic saturation with aprotic dodecane and protic brine ($S_{w,irr}$)

1. Different liquids in different pores

We show in Sec. III D that the most promising results of the presented methodology lie in the diphasic case of carbonates saturated with both brine and dodecane [Fig. 3(a)]. We have displayed in Fig. 6(a) the theoretical NMRD of both aprotic dodecane [Eqs. (6) and (7)] and protic water [Eqs. (8)–(10)] liquids calculated with the two different specific surface areas found above. These curves correspond to the best fits of the experimental data in Fig. 3(a). The small pores (R_{12}) exhibit the typical NMRD signature of wetting protic water [Eqs. (8)–(10)], whereas the large pores (R_{11}) have the typical NMRD signature of aprotic dodecane with weak surface affinity [Eqs. (6) and (7)]. This proves the separability of each surface NMRD pattern in Eq. (1). In particular, the good correspondence between Figs. 3(a) and 6(a) proves that the weak surface affinity index $A\sim130$ is preserved for R_{11} and the other index $B\gg1$ for R_{12}. These results reveal a clear identification of the nature of the different liquids saturating the dual porosity of carbonate [Fig. 3(b)].

2. Diphasic saturation in the same pore in the condition of mixed wettability

Lastly, we have displayed in Fig. 6(b) the calculated NMRD profiles when considering the case of aprotic and protic liquids in the same pore. These profiles have been obtained by the superposition of Eqs. (6)–(10) giving

$$\frac{1}{T_1(\omega_I)} = \frac{1}{T_{1,bulk}} + \frac{\pi}{30}\frac{N_{surface}}{N}\langle\omega_d^2\rangle\tau_m\left\{3\ln\left[\frac{1+\omega_I^2\tau_m^2}{(\tau_m/\tau_s)^2+\omega_I^2\tau_m^2}\right]+7\ln\left[\frac{1+\omega_S^2\tau_m^2}{(\tau_m/\tau_s)^2+\omega_S^2\tau_m^2}\right]\right\}$$
$$+\frac{2}{15}\frac{N_{param}}{N}\omega_{d,IS}^2 T_{1,elec}(\omega_S)\{3/[1+\omega_I^2T_{1,elec}^2(\omega_S)]+7/[1+\omega_S^2T_{1,elec}^2(\omega_S)]\}. \qquad (11)$$

This could correspond to a situation of a mixed wettability. These theoretical results show the logarithmic behavior at low frequency characteristic of the 2D diffusion at pore surfaces of aprotic dodecane and the net increase of the relaxation rate at high frequency due to the nuclear paramagnetic relaxation of the wetting protic brine. So, even in this complicated mixed wettability condition, the NMRD data could potentially identify the nature of the two different liquids saturating a given pore.

V. CONCLUSION

We have presented an *in situ* method for estimating wettability of oil and brine at the pore surfaces of rocks. It is based on nuclear magnetic relaxation dispersion (NMRD): the measurement of proton spin-lattice relaxation rates as a function of magnetic-field strength or nuclear Larmor frequency. This method separates wetting from nonwetting fluids through typical NMRD features due to their respective surface dynamics. This method has been applied to carbonate rocks representing about two thirds of the world's oil known reserves. The *in situ* results obtained on carbonates of bimodal porosity saturated with an oil/brine mixture unambiguously reveal the pore-size dependence of wettability. We have introduced a microscopic dynamical surface affinity index which measures the dynamical correlation (i.e., the microscopic wettability) between the diffusive fluid and the fixed relaxation sources at the pore surfaces. For aprotic liquid, the affinity index that varies between 1 (bulk) and infinity (strong surface affinity) allows to quantify the degree of dynamical correlation with the paramagnetic impurities present at the pore surface. The question becomes different for protic liquid due to the binding to the paramagnetic ions. However, one could define a similar index by comparing the time of residence on the paramagnetic ions to the electronic spin-lattice relaxation time. Based on our results, the method can be applied to *in situ* characterization of wettability of liquids confined in any other disordered porous media.

ACKNOWLEDGMENTS

We thank P. Levitz and D. Petit (PMC, Ecole Polytechnique) for stimulating discussions, S. Saner (Schlumberger, Dhahran) for polarized optical microscopy data, M. Hurlimann (Schlumberger, Boston), and B. Montaron (Schlumberger, Dubai) for useful discussions.

APPENDIX A: CALCULATION OF THE DIPOLAR CORRELATION FUNCTIONS $G_L^{(m)}(\tau)$ AND SPECTRAL DENSITIES $J_L^{(m)}(\omega)$

We outline in this appendix the main steps of the calculations of the pairwise dipolar correlation functions $G_L^{(m)}(\tau)$ and spectral densities $J_L^{(m)}(\omega)$ of an aprotic liquid diffusing at proximity of the pore surface. For further technical details about the integrations see Ref. [14].

Let us start from the integral average of the dipole-dipole interaction over the propagator of diffusion given in the laboratory frame (L) by Eq. (5):

$$G_L^{(m)}(\tau) = \int d\vec{r}_0 p(\vec{r}_0) F_L^{(-m)}(0) \int d\vec{r} P(\vec{r}_0, \vec{r}, \tau) F_L^{(-m)*}(\tau). \quad \text{(A1)}$$

We give below the four main steps that allow us to calculate Eq. (A1).

(i) We use the well known properties of rotation of spherical harmonics in different bases to facilitate the calculations in the lamellar frame (M) of Fig. 4 before coming back to the laboratory frame (L) associated to the constant direction of the magnetic field $\boldsymbol{B_0}$. This gives

$$G_L^{(m)}(\tau) = \sum_{m'=-2}^{+2} |d^{(2)}_{-m',m}(\beta)|^2 G_M^{(m')}(\tau), \quad \text{(A2)}$$

where the $d^{(2)}_{-m,m'}(\beta)$ are the well known Wigner functions [24] that allow to express the dipolar interaction $F_L^{(m)}(t)$ as it comes through a succession of coordinate rotations in the different frames $(M) \rightarrow (L)$ and $G_M^{(m')}(\tau)$ with $\{m' \in (-2, +2)\}$ are the pairwise dipolar correlation functions in the lamellar frame (M). These latter functions are given by an integral average over the propagator of diffusion in the lamellar frame (M) formally similar to Eq. (A1).

(ii) We use the anisotropic dynamical model presented in Fig. 4 with an unbounded and isotropic diffusion perpendicular to the normal axis $\boldsymbol{n}$ and a bounded diffusion along such an axis. When considering translational diffusion of the I-spin-bearing molecules in the quasi-two-dimensional geometry of Fig. 4, the anisotropy of the dynamics is described by an unbounded and isotropic (independent of φ) diffusion perpendicular to the normal axis $\boldsymbol{n}$ and a bounded diffusion along such an axis. According to this model, the normalized diffusive propagator P in the lamellar frame (M) is thus defined as a product of a bounded $P_\parallel$ and an unbounded $P_\perp$ term,

$$P(\rho, z, \tau | \rho_0, z_0, 0) = P_\perp(\rho, \tau | \rho_0, 0) P_\parallel(z, \tau | z_0, 0). \quad \text{(A3)}$$

The bounded propagator $P_\parallel$ is given by the solution of a 1D-diffusive equation with no flux out of the layer. The Gaussian unbounded propagator $P_\perp$ is expressed by its Fourier transform in the reciprocal k space [25]:

$$P_\parallel(z, \tau | z_0 0) \approx \frac{1}{\lambda}[1 + 2\cos(\pi z/\lambda)\cos(\pi z_0/\lambda)\exp(-D_{I\parallel}\tau/\lambda^2) + \cdots], \quad \text{(A4a)}$$

$$P_\perp(\rho, \tau | \rho_0, 0) = \frac{1}{2\pi} \sum_{m=-\infty}^{+\infty} \int_0^\infty dk\, k \exp(-k^2 D_{I\perp}\tau) J_m(k\rho) J_m(k\rho_0) \exp[im(\varphi_0 - \varphi)]. \quad \text{(A4b)}$$

Here $D_{I\parallel}$ and $D_{I\perp}$ are the translational diffusion of spins I in direction parallel and perpendicular to $\boldsymbol{n}$ and the $J_m(k\rho)$ are cylindrical Bessel functions of integer order m.

(iii) We are only interested in the situations encountered at long times $\tau\to\infty$ (or low frequency). In Eq. (A4a), $P_{\parallel}$ thus simplifies to the inverse of the "volume" $(1/\lambda)$ visited within the boundary conditions of zero flux along the $\boldsymbol{n}$ direction on the two limits of the layer of size I [25]. In Eq. (A4b), only the long wavelength transverse diffusing modes dominate $(k\to 0)$ for time τ much longer to the transverse diffusion correlation time: $\tau_m=\delta^2/(4D_{I\perp})$, where δ is the mean molecular size of the I-spin-bearing molecule. The propagator of diffusion in the lamellar frame, $P(\rho,z,\tau|\rho_0,z_0,0)=P_{\perp}(\rho,\tau|\rho_0,0)P_{\parallel}(z,\tau|z_0,0)$, is then substituted in the integral definition of $G_M^{(m')}(\tau)$ with $\{m'\in(-2,+2)\}$, giving at long times $(\tau\gg\tau_m)$:

$$G_M^{(m')}(\tau)=\frac{2\pi\sigma_S}{\lambda^2}\int_0^{\infty}dkk\,\exp(-k^2D_{I\perp}\tau)\times\left|\int dz\int d\rho\rho J_m(k\rho)f_2^{(m')}(\rho,z)\right|^2, \quad \text{(A5)}$$

where $f_2^{(m)}\sim 1/r_{IS}^3$ are the dipolar terms expressed in the cylindrical frame (Fig. 4). We have introduced in the calculations the distance of minimal approach δ' between spins I and S at pore surface (Fig. 4). Typically δ' is comparable to the molecular diameter δ. However, we have introduced below a parameter $x=\delta/\delta'$ in order to take into account a variable distance of minimal approach at proximity of the spin S. We have separated the integral calculations in Eq. (A5) into two domains: $M_1=\{\delta'\le z\le\lambda \text{ and } 0\le\rho<\infty\}$ and $M_2=\{0\le z\le\delta' \text{ and } \delta'\le\rho<\infty\}$ in the layer frame M (Fig. 4). The calculation of integrals simplify for times τ much longer than the two-dimensional correlation time τ_m. This approximation allows considering only the dominant term coming from the long wavelength two-dimensional transverse modes $k\delta'\to 0$ when $\tau\gg\tau_m$ in the exponential part $\exp[-(k\delta')^2x^2\tau/(4\tau_m)]$ of Eq. (A5). After some calculations, one finds that the leading terms come from the two-dimensional part of $G_M^{(0)}(\tau)$ integrated in the M_2 domain:

$$G_M^{(0)}(\tau)\approx\frac{3\pi\sigma_S}{4\lambda^2\delta'^2}\frac{1}{x^2}\left(\frac{\tau_m}{\tau}\right)+\vartheta[(\tau_m/\tau)^{3/2}], \quad \text{(A6a)}$$

$$G_M^{(1)}(\tau) \text{ and } G_M^{(1)}(\tau)\approx\vartheta[(\tau_m/\tau)^2]. \quad \text{(A6b)}$$

So, at long times and in the low-frequency range studied, only $G_M^{(0)}(\tau)$ matters.

It is physically interesting to represent $G_M^{(0)}(\tau)$ as

$$G_M^{(0)}(\tau)\approx\frac{3\pi^2}{4}\left(\frac{\sigma_S}{\lambda}\right)\left(\frac{1}{V(\tau)}\right), \quad \text{(A7a)}$$

where we introduce the volume of the cylinder $V(\tau)$ explored by the quasi-two-dimensional diffusion in a time τ in the layer frame (M) (Fig. 4):

$$V(\tau)=\pi(4D_{I\perp}\tau)\lambda. \quad \text{(A7b)}$$

Equations (A7a) and (A7b) thus become quasisimilar to the prefactor of a Gaussian probability for diffusion. This proves that, at long times, the pairwise dipolar correlation function $G_M^{(0)}(\tau)$ is clearly proportional to the probability of a reencounter between I and S spins by a two-dimensional diffusion in a given time τ.

(iv) However, to be a dipolar correlation function $G_M^{(0)}(\tau)$ must fulfill also the three following requirements [19]. (a) At short times, when $\tau\to 0$, $G_M^{(0)}(\tau)$ must tend to a finite constant C, such as $G_M^{(0)}(0)=\int_{-\infty}^{\infty}J_M^{(0)}(\omega)d\omega=C$, where $J_M^{(0)}(\omega)$ is the spectral density given by the Fourier transform of $G_M^{(0)}(\tau)$. (b) Equation (A6a) shows that, at long times, $G_M^{(0)}(\tau)$ must behave as a power law $1/\tau$ characteristic of a dipolar intermolecular relaxation process by a two-dimensional translational diffusion. Here we simply include the effect of the finite time of residence τ_S at pore surface by an exponential cutoff: $G_M^{(0)}(\tau)\propto(C/\tau)\exp(-\tau/\tau_S)$. (c) We must also consider the form of $G_M^{(0)}(\tau)$ on the time scale of surface molecular diffusion events, $0\le\tau\sim\tau_m\ll\tau_S$, characterized by the correlation time for the surface diffusion events. Finally all these requirements lead to the following expression of the correlation function $G_M^{(0)}(\tau)$ which is, as expected, always positive:

$$G_M^{(0)}(\tau)\approx C\frac{\tau_m}{\tau}\left[\exp\left(-\frac{\tau}{\tau_S}\right)-\exp\left(-\frac{\tau}{\tau_m}\right)\right] \text{ when } \tau_m\ll\tau_S. \quad \text{(A8)}$$

Straightforward calculations give $C=3\pi\sigma_S/(4x^2\lambda^2\delta'^2)$. The spectral density function is thus given by the exponential Fourier transform of Eq. (A8):

$$J_M^{(0)}(\omega)=\frac{3\pi\sigma_S}{4x^2\lambda^2\delta'^2}\tau_m\ln\left[\frac{1+\omega^2\tau_m^2}{(\tau_m/\tau_S)^2+\omega^2\tau_m^2}\right]. \quad \text{(A9)}$$

(v) Last, we make a powder average of $J_M^{(m)}(\omega)$ over all the orientations β of the (M) frame relative to the constant direction of $\boldsymbol{B}_0$ and obtain the average spectral densities:

$$\langle J_L^{(0)}(\omega)\rangle=\langle J_L^{(1)}(\omega)\rangle=\langle J_L^{(2)}(\omega)\rangle\approx\frac{1}{5}J_M^{(0)}(\omega). \quad \text{(A10)}$$

Substitution of Eq. (A9) into Eq. (A10) gives finally the powder average of the spectral density in the laboratory frame (L):

$$\langle J_L^{(m)}(\omega)\rangle=\int_{-\infty}^{+\infty}\langle G_L^{(m)}(\tau)\rangle e^{-i\omega\tau}d\tau=\frac{3\pi\sigma_S}{20x^2\lambda^2\delta'^2}\tau_m\ln\left[\frac{1+\omega^2\tau_m^2}{(\tau_m/\tau_S)^2+\omega^2\tau_m^2}\right]. \quad \text{(A11)}$$

APPENDIX B: EFFECT OF CONCENTRATION OF PARAMAGNETIC SITES

The mass concentration of paramagnetic sites of rock samples is obtained by crushing the dry material in small

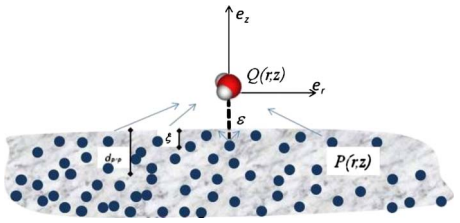

FIG. 7. (Color online) Schematic representation of the influence of a distribution of paramagnetic sites $P(r,z)$, on a proton located at $Q(r,z)$, at a distance ε from the grain interface. At this scale the grain (size of several microns) is supposed to be a flat surface (its curvature is much larger than ε).

particles and use of a calibrated ESR described in the text. The average distance between two paramagnetic sites P and P' (Mn^{2+} ions for instance) located on corners of an elementary cube (Fig. 7) is given by the cubic root of the inverse of the volumic concentration:

$$d_{P'P} = \frac{1}{(\rho_S \eta_S)^{1/3}}. \tag{B1}$$

This distance does not reflect the actual concentration of the acting sites in the vicinity of a pore rock grain. The real sphere of influence of a single paramagnetic site on a moving proton depends on the paramagnetic relaxation rate [Eq. (8)] whose maximum value is $\frac{2}{15}\omega_{d,IS}^2$ representing the interaction between a proton-water and a given Mn^{2+} ion at a distance of minimal approach $\delta' = 0.27$ nm. The spatial influence of the paramagnetic ions on the nuclear relaxation of a moving proton (Fig. 7) is expressed as a function of the distance r_{PQ} as a dipolar influence, i.e., inversely proportional to the sixth power of the distance. The maximal influence is obtained for the distance of minimal approach $\delta' = 0.27$ nm when the proton belongs to the ligand field of the Mn^{2+} paramagnetic ions:

$$\omega_{d,PQ}^2 = \left(\frac{\gamma_I \gamma_S \hbar}{r_{PQ}^3}\right)^2 S(S+1) = \omega_{d,IS}^2 \frac{\delta'^6}{r_{PQ}^6}. \tag{B2}$$

When the a-dimensional distance r_{PQ}/δ' doubles, the amplitude of the influence is divided by 64; when it triples, it is divided by 729 meaning that the influence of a paramagnetic site is very singular.

We now express the collective effect $K(\varepsilon)$ of all paramagnetic sites dispersed in the solid on a proton located at a distance ε from the grain surface (Fig. 7). The two sites are distant of $[r^2+(z+\varepsilon)^2]^{1/2}$ from the proton at the control point $Q(0,\varepsilon)$. This influence is expressed by the integral over the volume of the grain (extended to infinity since far influence becomes null) and weighted by the volume concentration of paramagnetic sites $\eta_S \rho_S$:

$$K(\varepsilon) = 2\pi A \eta_S \rho_S \int_{z=0}^{\infty} dz \int_{r=0}^{\infty} \frac{r dr}{[r^2+(z+\varepsilon)^2]^3} = \frac{\pi A \eta_S \rho_S}{6\varepsilon^3}, \tag{B3}$$

where $A = \omega_{d,IS}^2 \delta'^6$. A critical distance ε_c is obtained when the importance of a single paramagnetic site is balanced by the collective effect of all:

$$\frac{A}{\varepsilon_c^6} = \frac{\pi A \rho_s \eta_S}{6\varepsilon_c^3} \Leftrightarrow \varepsilon_c = \left(\frac{6}{\pi \rho_s \eta_S}\right)^{1/3} = \frac{1.24}{(\rho_s \eta_S)^{1/3}} = 1.24 d_{P'P}. \tag{B4}$$

For a uniform distribution of the site in the matrix, ε_c is very close to the average distance $d_{P'P}$ defined in Eq. (B1). The concentration of paramagnetic is measured by ESR as $\eta_S = 8.4 \times 10^{19}$ Mn^{2+}/g equivalent to $\rho_S \eta_S = 2.1 \times 10^{20}$ Mn^{2+}/cc leading to $d_{P'P} \approx 1.7$ nm $\approx 6.3\delta'$. Since the effect of $d_{P'P}$ of a single paramagnetic site decreases like the sixth power of the distance, this concentration shows an influence factor on the order of 1.6×10^{-5} of the maximal influence at δ'. To get significant interaction of adjacent sites, we should have much higher concentration of manganese ions. This proves that each ion acts individually validating the hypothesis of dispersed spinning sites. In this frame the surface concentration of sites in a band of thickness $d_{P'P}$ at the grain surface is on the order of the volume concentration of the ions multiplied by the thickness $d_{P'P}$. The depth of each ion is a random value in the range $z \in \{0, -d_{P'P}\}$. The probability of the ions to be at the surface $z=0$ or either deeply buried $z=-d_{P'P}$ is assumed to be uniform in the rock grain. Among all the sites in this layer, only the one closest to the surface of the pore will be active on the moving proton species. In order to define the effective depth of concerned ions we define an arbitrary level of influence for instance such as the amplitude of $\omega_{d,IS}^2$ is greater than a given sensitivity factor $\zeta = 1\%$ (for instance) of its maximal amplitude $\omega_{d,IS_{\max}}^2$. Using Eq. (B2), we obtain

$$\zeta = \frac{\omega_{d,PQ}^2}{\omega_{d,IS}^2} = \left(\frac{\delta'}{\xi}\right)^6 \Leftrightarrow \xi = \frac{\delta'}{\zeta^{1/6}} = \begin{vmatrix} 0.50 \text{ nm} & (\zeta = 0.025) \\ 0.60 \text{ nm} & (\zeta = 0.010) \\ 0.85 \text{ nm} & (\zeta = 0.001) \end{vmatrix}. \tag{B5}$$

The effective layer ξ is much smaller than $d_{P'P}$; the effective surface concentration σ_S thus becomes

$$\sigma_S = \eta_S \rho_S \xi = \frac{\delta'}{\zeta^{1/6}} \left(\frac{1}{\eta_S \rho_S}\right)^{1/3} \approx 1.05 \times 10^{13} \ Mn^{2+}/cm^2 \tag{B6}$$

calculated with $\xi \sim 0.5$ nm. We choose such an effective layer ξ because it corresponds exactly to the lattice constant of the calcium carbonate lattice structure on which the Mn^{2+} ions are substituted to a few Ca^{2+} ions. The average distance $1/\sqrt{\sigma_S} \approx 3.1$ nm between two Mn^{2+} within such a layer is much larger than the lattice constant 0.5 nm of the calcium carbonate lattice, thus, justifying the isolate spin environment and the typical six-peak hyperfine ESR spectrum observed. We use this value of σ_S in the fits of Eqs. (6), (7), and (10) in Secs. III A–III C.

Now let us consider the effect of nonhomogeneities in the distribution of the paramagnetic sites. Since the sites are statistically dispersed their average distributions are made on the sum of individual isolated sites:

$$K(\varepsilon) = 2\pi A \eta_S \rho_S \int_{z=0}^{\infty} dz \int_{r=0}^{\infty} \frac{P(r) r dr}{[r^2 + (z+\varepsilon)^2]^3}. \quad \text{(B7)}$$

Here $P(r)$ is the spatial distribution of the sites located in the rock matrix. If this distribution is made of discrete elements $P(r) = \Sigma_{N_{sites}} \delta_{ac}(r - r_i)$ located at the random locations i in the medium. If the summation is made over the entire domain, the linearity of Eq. (B7) with respect to the distribution factor allows using the average as the resulting value. It may be possible that aggregates of ions exist and the relaxation will be different in this case. But the ESR spectrum will be completely different.

[1] E. R. T. Donaldson and P. Lorenz, SPE J. **9**, 13 (1969).
[2] W. G. Anderson, JPT, J. Pet. Technol. **38**, 1125 (1986).
[3] M. Robin, Oil Gas Sci. Technol. **56**, 55 (2001).
[4] R. Salathiel, JPT, J. Pet. Technol. **25**, 1216 (1973).
[5] W. G. Anderson, JPT, J. Pet. Technol. **39**, 1605 (1987).
[6] E. Amott, Trans. AIME **216**, 156 (1959).
[7] A. Dixit, J. Buckley, S. McDougall, and K. Sorbie, Transp. Porous Media **40**, 27 (2000).
[8] W. J. Looyestijn, Petrophys. **49**, 130 (2008).
[9] M. Fleury and F. Deflandre, Magn. Reson. Imaging **21**, 385 (2003).
[10] J. Chen, G. J. Hirasaki, and M. Flaum, J. Pet. Sci. Eng. **52**, 161 (2006).
[11] F. Noack, Prog. Nucl. Magn. Reson. Spectrosc. **18**, 171 (1986).
[12] R. Kimmich and E. Anoardo, Prog. Nucl. Magn. Reson. Spectrosc. **44**, 257 (2004).
[13] M. D. Hurlimann, L. Venkataramanan, and C. Straley, U.S. Patent No. 6,883,702 (2005).
[14] J. P. Korb, M. Whaley-Hodges, and R. G. Bryant, Phys. Rev. E **56**, 1934 (1997).
[15] S. Godefroy, J. P. Korb, M. Fleury, and R. G. Bryant, Phys. Rev. E **64**, 021605 (2001).
[16] BP, S.R.O.W.E. (ed.bp.com/statisticalreview) (2008).
[17] S. Fujiwara, Proc. Anal. Div. Chem. Soc. **36**, 2259 (1964).
[18] E. Barberon, J. P. Korb, D. Petit, V. Morin, and E. Bermejo, Phys. Rev. Lett. **90**, 116103 (2003).
[19] A. Abragam, *The Principles of Nuclear Magnetism* (Clarendon, Oxford, 1961).
[20] J. J. Fripiat, M. Letellier, P. Levitz, and J. M. Thomas, Philos. Trans. R. Soc. London, Ser. A **311**, 287 (1984).
[21] I. Solomon, Phys. Rev. **99**, 559 (1955).
[22] N. Bloembergen and L. O. Morgan, J. Chem. Phys. **34**, 842 (1961).
[23] J. P. Korb, G. Diakova, and R. G. Bryant, J. Chem. Phys. **124**, 134910 (2006).
[24] D. A. Varshalovich, A. N. Moskalev, and V. K. Khersonkii, *Quantum Theory of Angular Momentum* (World Scientific, Singapore, 1988).
[25] H. S. Carslow and J. C. Jaeger, *Conduction of Heat in Solids* (Clarendon, Oxford, 1959).